PAPER

A Compact Autonomous Underwater Vehicle With Cephalopod-Inspired Propulsion

AUTHORS

Zhuoyuan Song
Cameron Mazzola
Department of Mechanical and Aerospace Engineering, University of Florida

Eric Schwartz
Ruirong Chen
Department of Electrical and Computer Engineering, University of Florida

Julian Finlaw
Mike Krieg
Department of Mechanical and Aerospace Engineering, University of Florida

Kamran Mohseni
Departments of Mechanical and Aerospace Engineering, Electrical and Computer Engineering, and Institute for Networked Autonomous Systems, University of Florida

ABSTRACT

In this paper, a bioinspired, compact, cost-effective autonomous underwater vehicle system is presented. Designed to operate in a heterogeneous, multivehicle collaboration hierarchy, the presented vehicle design features 3D printing technology to enable fast fabrication with a complex internal structure. Similar to a previous vehicle prototype, this system generates propulsive forces by expelling unsteady, pulsed jets, inspired by the locomotion of cephalopods and jellyfish. The novel thrusters enable the vehicle to be fully actuated in horizontal plane motions, without sacrificing the low-forward-drag, slender vehicle profile. By successively ingesting water and expelling finite water jets, periodic actuation forces are generated at all possible vehicle velocities, eliminating the need for control surfaces used in many conventional underwater vehicle designs. A semiactive buoyancy control system, inspired by the nautilus, adjusts the vehicle depth by passively allowing water flowing into and actively expelling water out of an internal bladder. A compact embedded system is developed to achieve the control and sensing capabilities necessary for multiagent interactions with the minimum required processing power and at a low energy cost. The new vehicle design also showcases an underwater optical communication system for short-range, high-speed data transmission, supplementing the conventional acoustic communication system. Experimental results show that, with the thruster motors powered at a 60% duty-cycle, the new vehicle is able to achieve a 1/4 zero-radius turn in 3.5 s and one-body-width sway translation in 2.5 s.

Keywords: AUV, propulsion, bioinspired, optical communication, multivehicle collaboration

Introduction

Marine robotics has a significant impact on many related fields of research including marine ecology (Clark et al., 2013), oceanography (Fernandes et al., 2000; Eriksen et al., 2001; Grasmueck et al., 2006), and oceanic meteorology (Chao et al., 2008). Many design aspects of existing underwater robots were inspired by marine organisms that have been dominating the ocean for centuries. The unique sensing capabilities and locomotion efficiency of these marine organisms allow them to robustly adapt to the highly inhospitable ocean environment. To this end, multiple bioinspired designs have been proposed in order to improve the capability and performance of marine robots, including hydrodynamic-efficient locomotion (Palmre et al., 2013; Krieg & Mohseni, 2015), long-range acoustic communication, and multimodal sensing (Xu & Mohseni, 2014; DeVries et al., 2015).

Among many bioinspired marine robotic innovations, resilient, adaptive underwater actuation is one of the most studied topics (Chu et al., 2012). Besides traditional actuation methods relying on rigid driving mechanisms, the new field of soft robotics has motivated several efforts in studying the actuation mechanisms of marine animals such as cephalopods (Weymouth et al., 2015; Giorgio-Serchi et al., 2016). Unlike ground mobile robots, the locomotion of a marine vehicle is tightly coupled with the movements of a surrounding fluid. This dynamic interplay necessitates a thorough understanding of the interactions between moving thruster structures and the fluid motions produced. One distinct characteristic of small autonomous underwater vehicles

(AUVs) is their highly limited onboard power supply, which poses stringent design requirements on the total energy available for propulsion/maneuvering in order to elongate the overall vehicle endurance. For the same reason, agile maneuverability is also highly preferable to prevent redundant actuation during station-keeping and disturbance rejection.

Our group has studied the propulsion mechanisms of jellyfish, squid, and other cephalopods (Mohseni, 2006; Sahin & Mohseni, 2009; Lipinski & Mohseni, 2009; Krieg et al., 2015; Sledge et al., 2015), which all share as a common element a periodic pattern of expelling high-momentum, finite, propulsive jets followed by a refilling phase. Though this propulsive mechanism has historically been considered inefficient, based on steady-state scaling laws (Lighthill, 1969), recent studies on various developmental stages of squid have suggested that high-momentum propulsive jets may not necessarily negate a high propulsive efficiency (Bartol et al., 2008, 2009). Therefore, finite, propulsive jets may be more of a feasible option for underwater vehicle locomotion than previously thought. One aspect of squid and jellyfish swimming is an ability to create impulsive movements with impressive acceleration. Such an ability would clearly be an advantage in underwater robotics. We have shown, utilizing prototype thrusters inspired by squid and jellyfish, that, in fact, pulsed jet thrusters reach their desired thrust output nearly instantaneously (Krieg & Mohseni, 2010), unlike traditional, propeller-style thrusters, which can take several seconds to reach the desired level of thrust (Yoerger et al., 1990; Fossen, 1994).

Another advantage of the squid/jellyfish-inspired propulsion is that an external fluid manipulator is not required; the propulsion is generated from an internal jetting cavity, much like the internal mantle cavity of squid and octopus. As such, this style of propulsion can enable low-speed maneuvering capabilities like sideways translation (sway) and zero-radius turning (yaw) on slender, low-drag, torpedo-shaped vehicles, which otherwise would be lacking in low-speed maneuvering (Mohseni, 2006; Krieg & Mohseni, 2008, 2010). The most sophisticated of a series of vehicles employing this type of maneuvering was named CephaloBot, summarized in Krieg et al. (2011), that has full control authority in planar motions, both acoustic and image-based sensing capabilities, and significant processing capabilities.

In addition to their fast time response, the squid/jellyfish-inspired thrusters do not add extruding structures to a low-drag vehicle profile. Such structures would increase the overall vehicle drag in forward motion, much like propeller-based thrusters added to underwater vehicles, such as remotely operated vehicles, that require accurate, low-speed maneuvering. The outcomes of this include total elimination of control surfaces on the vehicle and fully decoupled horizontal vehicle movements. These features make our vehicles more suitable for various real-world applications (e.g., station keeping, navigation in confined spaces, and parallel parking) that are difficult for conventional AUVs with control surfaces to accomplish. In addition, fully actuated horizontal vehicle dynamics significantly simplifies the design of vehicle control algorithms such as path planning, trajectory following, and disturbance rejection.

The goal of this paper is to describe the adaptations made to develop a new generation of bioinspired AUVs that are highly cost-effective and much smaller in size. This new design is necessitated by a mother-daughter, hierarchical, multivehicle cooperative system. Such a multivehicle hierarchy is motivated by the ever-increasing demands for large-scale, *in-situ*, oceanic sensing and data collection, which have been significantly benefiting marine meteorology, weather prediction, ocean modeling, etc. (Leonard et al., 2007; Howe et al., 2010; Das et al., 2012; Michini et al., 2014; Reed & Hover, 2014). Large numbers of sensor nodes are typically required to provide comprehensive spatial coverage. The new AUV design presented in this article is to serve such a purpose while preserving the preferable mobility of AUVs when compared to conventional ocean drifters and floats (D'Asaro, 2003; Roemmich et al., 2009).

Cost-effectiveness of underwater mobile sensor nodes is usually achieved by sacrificing their sensing, processing, and actuation capabilities. One critical challenge faced by these mobile sensor nodes is the fast degeneration of navigation performance. Due to a lack of expensive navigation sensors (e.g., DVL and sonar), these platforms heavily depend on low-cost inertial navigation systems and frequent, time-consuming surfacing for navigation error corrections. However, accurate localization is essential for the sensor nodes to effectively execute collaborative data collection algorithms and georeferencing the obtained data of interest. Long-term, accurate navigation is crucial to mobile sensor platforms in order to improve their sensing quality and efficiency.

Cooperative multivehicle systems are advantageous in overcoming the limitations of sensor accuracy, processing capability, coverage, and efficiency of low-cost AUVs. The mother-daughter,

multivehicle hierarchy is aimed at improving the overall navigation performance of daughter vehicles, serving as cost-effective mobile sensor nodes, with a small number of well-equipped mother vehicles, performing higher-level decision making, data processing, and navigational drift corrections. The high-quality navigation sensors onboard mother vehicles enable them to maintain bounded navigation errors. These vehicles can serve as suboptimal navigation references for cost-effective daughter vehicles through intervehicle communication and relative position measurements. Meanwhile, mother-daughter interactions can also facilitate *in-situ* sensor data collection and task distribution.

We showcase our most recent design of a daughter vehicle prototype. This vehicle is equipped with one rear propeller to provide forward thrust and four lateral bioinspired squid actuators to enable agile slow-speed maneuvering. We start by introducing the fundamental multivehicle navigation structure, which poses high-level design requirements for the daughter vehicles. New realizations of energy-optimal driving programs, which have recently been implemented in our bioinspired thrusters, are then presented. Driven by the objective of cost-effectiveness and fabrication simplicity, we present an AUV design incorporating 3D printing technology. A simple buoyancy control system, inspired by marine animals such as the nautilus, is developed. The compact embedded system coordinating actuator movements and sensor inputs is discussed. We equipped the daughter vehicle prototype with an optical communication system to supplement the acoustic communication system and handle short-range, high-speed data transmission with mother vehicles. The maneuverability of the presented AUV design is demonstrated with experiment results. We conclude this paper with a discussion on potential improvements in cost-effective AUV designs.

Hierarchical Multi-AUV System

The mother-daughter, multi-AUV system comprises one or more well-equipped AUVs, dubbed mother AUVs (MAUVs), and many cost-effective vehicles, named daughter AUVs (DAUVs). The localization error of MAUVs can be bounded by a combination of high-performance navigation sensors on board. State estimation of DAUVs relies on dead-reckoning with noisy measurements of low-cost inertial navigation systems. Both types of AUVs are assumed to be capable of communicating with neighboring agents in the sensor range as well as obtaining the relative position information of their neighbors (Song & Mohseni, 2013). The benefit of such a hierarchical network to the navigation performance of DAUVs is threefold. Interactions among DAUVs enable exchange of location estimates under the cooperative localization framework (Bahr et al., 2009). The degeneration rate of inertial navigation performance can be decreased and the state estimation across the DAUV fleet becomes dependent. This facilitates the second benefit, which is that the navigation error divergence of DAUVs is further alleviated through incorporating information from MAUVs (Song & Mohseni, 2014). Another benefit of the hierarchical AUV network is that major planning, processing, and data storage can be managed by MAUVs, making it possible to build DAUVs with minimum processing capabilities.

In order to experimentally test and analyze the mother-daughter navigation hierarchy, we design the daughter vehicle prototype with agile maneuverability and basic state estimation and intervehicle communication capabilities. Using the mother-daughter hierarchy as our design guideline, we follow the same actuator placements as CephaloBot to maintain the decoupled horizontal maneuverability (see Figure 1). Supplementing a conventional acoustic communication modem responsible for routine information exchanges and exteroceptive sensing, the DAUV prototype showcases a compact, optical communication system for short-range, high-speed data transmission. This allows for fast transmission of large data packages between the DAUVs and either the MAUVs or a docking station.

Bioinspired Actuation

The jet propulsion mechanisms employed by marine invertebrates are fundamentally different from the continuous jet propulsion of recreational watercraft. These animals are not capable of continuously pumping fluid; instead, they must stop jetting periodically to refill an internal cavity driving jet expulsion. When a fluid jet is expelled in this fashion, starting from rest, the free shear tube created is unstable and rolls into a vortex ring. The vortex ring grows with increasing jet flow until a critical point is reached and its circulation becomes saturated, resulting in the ring separating from the remaining shear flow which forms a trailing wake (Gharib et al., 1998). Gharib et al. defined a normalized time scale called the formation time, $t_f = \int_0^t u_j \mathrm{d}t/D$, where u_j is the jet velocity and D is the nozzle diameter. They also showed that vortex ring "pinch-off" occurs at a

FIGURE 1

Fifth-generation hybrid vehicle CephaloBot (Krieg et al., 2011) as the MAUV (a, b) and the proposed compact design as the DAUV (c, d). For the DAUV (c, d), complex internal geometry such as the thruster mounts, buoyancy bag enclosure, and internal ribs are easily manufactured using 3D printing. The internal ribs increase the space inside the hull, and the thruster mounts and buoyancy bag enclosure help ease assembly. The rear propeller drive system is integrated with the vehicle using a magnetic coaxial coupling. The buoyancy system adjusts the buoyancy of the DAUV by allowing water to go in or pumping water out of the bladder. (Color version of figures are available online at: http://www.ingentaconnect.com/content/mts/mtsj/2016/00000050/00000005).

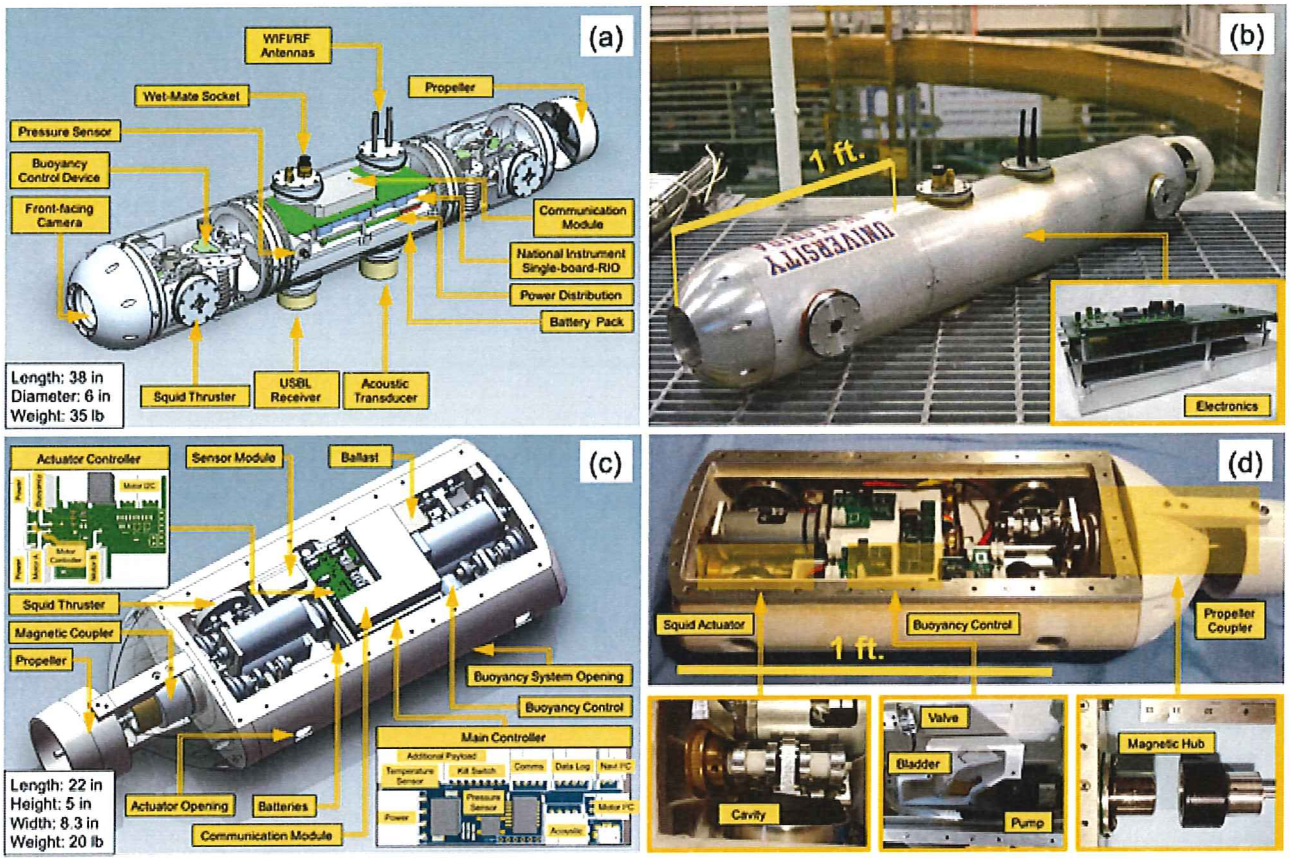

universal formation time, independent of nozzle diameter and jet velocity. If the jet is considered to be a solid cylinder then the ratio of its length to width, sometimes referred to as the stroke ratio of the jet (out of deference to cylinder piston style vortex generators used in several studies), is equal to the formation time. The universal formation time of vortex ring pinch-off, $t_f^* \approx 4$, is referred to as the formation number (Gharib et al., 1998). Vortex ring formation clearly plays a large role in biological jet locomotion since swimming behaviors can be categorized by whether the animal creates propulsive jets with stroke ratios either above or below the formation number. This is true for both jellyfish (Dabiri et al., 2005, 2010) and squid (Bartol et al., 2009).

Inspired by this method of marine invertebrate locomotion, we characterized the impulse transfer associated with unsteady jetting. It was determined that a converging radial velocity in the jet generated by funnel morphology in both squid and jellyfish, as well as by the formation of the primary vortex ring, increases both impulse transfer and circulation generated in the jet (Krieg & Mohseni, 2013) when compared with steady 2D jets with parallel streamlines. The thrust enhancement due to converging radial velocity induced by the formation of the primary vortex ring is maximized by jet stroke ratios near the formation number (Krieg & Mohseni, 2013) and can reach an increase of as much as 75% for flat-orifice nozzle geometries. In addition, testing of a prototype thruster, at pulsation frequencies only available to robotic reproductions, demonstrated that there

were significant losses in thrust when the jet stroke ratio was above the formation number due to reingestion of the jet trailing wake (Krieg & Mohseni, 2008). These losses increase with both increasing stroke ratio and increasing frequency. These features of unsteady jet dynamics drive the design of nozzle geometry and allow for an optimal correlation between nozzle geometry and jet volume in vehicle thruster models.

Squid, by far the fastest of the marine invertebrates, are known to eject jets with an impulsive velocity program. This means that both the jetting and refilling velocities are relatively constant with rapid velocity changes when switching between the two. Figure 2, taken from Anderson and DeMont (2000, Figure 5), shows the mantle volume of a squid vs. time for a typical cruising velocity. As can be seen in this figure, the rate of change of volume is nearly linear for both jetting and refilling phases with significant accelerations when changing directions of the flow.

In an effort to explain whether this behavior is motivated by morphology, maximum swimming velocity, or efficiency, we developed high-fidelity models for pressure inside the cavity during unsteady jetting, based on the evolution of circulation in the system (Krieg & Mohseni, 2015). It was demonstrated in this study empirically that less energy is required to produce jets with an impulsive velocity program. Two characteristic thruster jet velocity programs are discussed here. Figure 3a shows an impulsive velocity program where the thruster quickly accelerates to a desired velocity and then holds that velocity nearly constant throughout pulsation. Figure 3b shows a sinusoidal velocity program, where the jet velocity gradually increases and then decreases throughout the pulsation cycle. Figure 4 shows the energy required to create two propulsive jets with identical hydrodynamic impulse (propulsive output) and identical jetting periods, but with impulsive vs. sinusoidal jet velocity programs. Though it might be reasoned that the impulsive velocity program would increase the total required work since it requires such large accelerations at the onset of motion, the total required energy is lower because the large pressure forces due to acceleration coincide with minimal cavity deformation velocity (Krieg & Mohseni, 2015). The sinusoidal velocity program, on the other hand, results in maximum pressure forces due to momentum transfer that coincide with maximum jet velocity and maximum cavity deformation velocity. As such there is a much larger peak in required energy as can be seen in Figure 4b.

The discovery of an optimal jet velocity program with respect to propulsive efficiency was made after the most recent vehicle prototype and corresponding thrusters had already been designed, fabricated, and reported in Krieg et al. (2011). Fortunately, the mechanical design and geometry of the thrusters do not need to be altered for the vehicle to take advantage

FIGURE 3

Thruster jet velocity associated with impulsive (a) and sinusoidal (b) velocity programs.

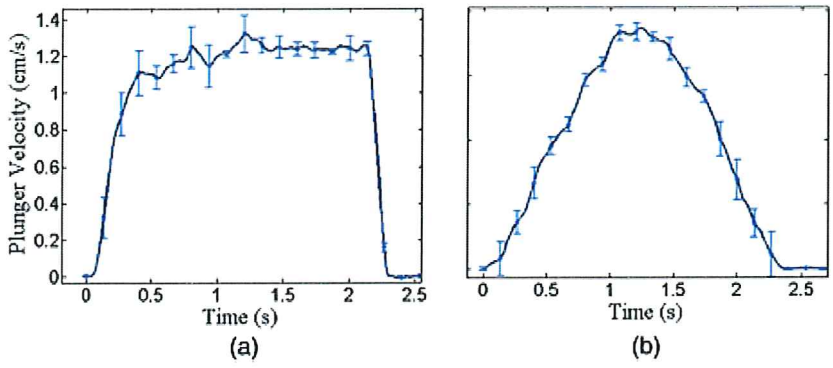

FIGURE 2

Mantle volume of *Loligo pealei* vs. time during the jetting process. Figure adapted from Figure 5 of Anderson and DeMont (2000), including straight lines to show the nearly linear volume flux program employed by squid.

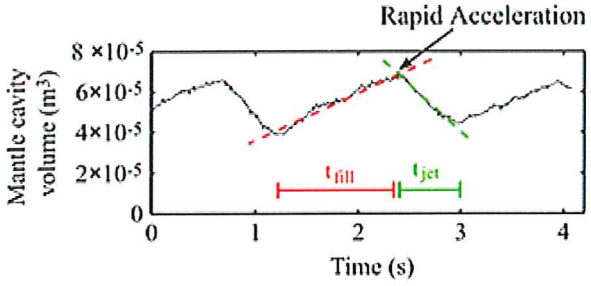

FIGURE 4

Instantaneous power required to drive plunger motion for (a) an impulsive plunger deflection and (b) a sinusoidal plunger deflection. Also the total work over the entire cycle is listed for each case. Data previously presented in Krieg and Mohseni (2015). (a) Total Required Energy = 0.31Nm. (b) Total Required Energy = 0.53Nm.

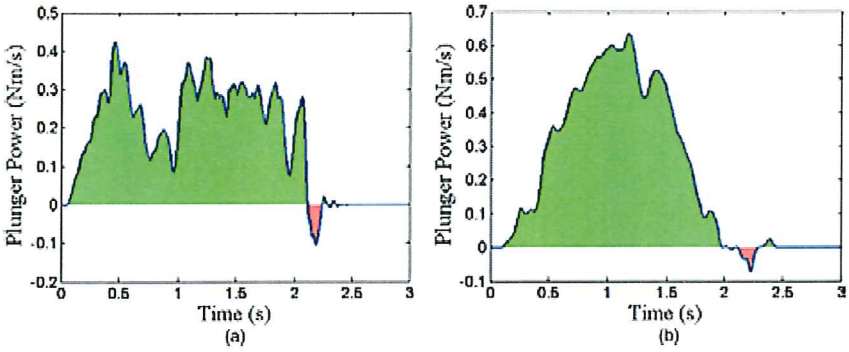

of the optimal velocity programs. The jetting velocity can be varied by the vehicle controller, so implementation only requires alteration of the controller driving programs. The new jetting velocity program has been implemented on the controller of the legacy vehicle reported in Krieg et al. (2011), as well as the new DAUV platform described in this work (see Figures 1c-1d).

Fast Vehicle Fabrication With 3D Printing Technology

It is highly desirable for an AUV to be easy to transport and deploy and also to have a greater range of access to constrained spaces. However, limited by conventional fabrication methods, it becomes a challenge in compact AUV designs to maintain comparable maneuverability and sensing capabilities with that of larger vehicles. To this end, the introduction of rapid prototyping methods, such as 3D printing, offers an appealing alternative to conventional subtractive manufacturing methods. The hull of the DAUV prototype was manufactured by a Fortus 360 mc rapid prototyping machine with an accuracy of ±0.0015 inch per inch. Polycarbonate was selected as the printing material due to its higher tensile strength than acrylonitrile butadiene styrene, which results in better structural integrity.

In general, the surface area of an AUV scales with some characteristic length-scale squared, and the volume is proportional to the length-scale cubed. This means that AUV surface area and volume change disproportionally as vehicle size is reduced. Therefore, relative to the drag forces that they must overcome, smaller vehicles have less internal volume to work with, which causes spatial optimization to become a high priority during the vehicle design process. Traditional manufacturing processes often cannot create the complex internal and external features desired in compact underwater vehicles. Computer numerical control (CNC) milling machines are able to produce some of these three-dimensional structures, but only with a large time and labor commitment. On the other hand, 3D printing allows complex features such as internal ribs and component-specific interfaces to be built directly into the vehicle hull (see Figures 1c-1d). This results in easier assembly as well as more usable internal space for payload and sensor hardware, which would otherwise be occupied by redundant hull materials that are difficult to remove by subtractive machining. Using 3D printing technology, the fabrication time for the daughter vehicle was decreased by approximately 75% compared to CNC machining.

The rear propeller drive system utilizes a magnetic coaxial coupling by Magnetic Technologies to transmit torque from a shaft inside the vehicle to an external propeller drive shaft without physical contact. A hollow containment barrier is fastened to the hull and protrudes aft towards the rear propeller. A magnetic hub fastened to the internal shaft resides inside the containment barrier, while a magnetic hub fastened to the external propeller shaft is positioned coaxially around the containment barrier. The two hubs maintain angular alignment due to magnetic attraction, which allows for torque transfer between the internal and external shafts.

Though there are many advantages of 3D printing technology compared to the conventional manufacturing techniques in AUV fabrication, several new design challenges are posed by 3D-printed underwater vehicles. The 3D-printed material is inherently not waterproof, even when printed at 100% infill, and must be post-processed. For the DAUV prototype, US Composites 635 thin epoxy resin system was used to coat the exterior of the hull. This low-viscosity epoxy provides a smooth, consistent, waterproof surface coating to the hull. One disadvantage is the brittle nature of the epoxy. After extended use, the epoxy

may chip off or delaminate from the surface of the hull. The epoxy does not seep into and impregnate the plastic, which is the main cause for potential delamination. Sealing external openings is one of the toughest challenges with 3D-printed underwater vehicles. Even with a smooth epoxy coating on top of the plastic surface, traditional gasket and O-ring sealing methods for the thrusters and removable top did not consistently seal the vehicle during initial testing. At these locations, flat aluminum plates are fastened onto the surface of the plastic hull to provide a smoother surface for a gasket interface, as seen in Figure 1d.

FIGURE 5

Illustration of the working principle of the buoyancy control system during the vehicle submerging phase and the vehicle surfacing phase (a) and the control board that coordinates the behavior of the pump and the valve (b).

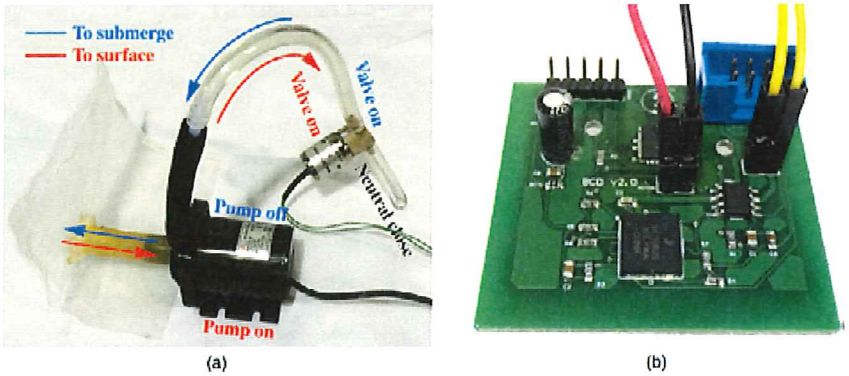

Buoyancy Control System

The DAUV prototype uses an internal bladder system that provides a change in vehicle buoyancy via a pump and valve configuration. This system mimics the depth control system of the nautilus, which makes daily trips to deeper waters for feeding. The nautilus draws water into and out of the living chamber through the hyponome in order to produce jet propulsion. The change of ion concentration within the chamber fluid is a result of osmosis via its siphuncle, which leads to changes in the volumes of water and gas within each of its shell chambers, resulting in buoyancy changes. Such a buoyancy system takes the advantage of the ion gradient to achieve effective depth adjustments.

Driven by the demand for a compact yet effective design, the buoyancy system of the DAUV consists of a pump and valve configuration to both passively intake and actively expel water from a buoyancy bag (bladder) inside the vehicle (see Figure 1d). A Parker Series-3 miniature inert valve controls the water flow going into and out of the buoyancy bag. The resting state of the valve is closed, which allows for power consumption to be minimized when depth changes are not needed. Water is allowed to flow into the buoyancy bag subject to the natural pressure gradient to decrease the buoyancy of the vehicle. A LightObject brushless submersible water pump, with a 5-m maximum head, pulls water from the bladder and forces it outside of the vehicle to increase the vehicle buoyancy. A gauge (absolute) pressure sensor is calibrated to provide instantaneous depth measurements, which is utilized by the buoyancy control feedback algorithm.

Figure 5a illustrates the working principle of this buoyancy system in more detail. The arrows indicate the direction of water flow in both the vehicle submerging phase and surfacing phase. The valve is neutrally closed in the absence of power. For the vehicle to submerge, the valve opens to allow water to flow through the unactuated pump into the water bag due to the natural pressure gradient. For the vehicle to surface, the valve opens and the pump activates to eject water from the water bag out of the vehicle to regain positive buoyancy. The coordination between the pump and the valve is controlled by the buoyancy system control board (Figure 5b).

Compact Embedded System

A modular embedded vehicle control system has been constructed in order to facilitate vehicle motion, record sensor readings, and communicate with the mother vehicle. This modular system consists of a main control printed circuit board (PCB) that directs motor operation via I^2C communication, as well as three slave PCBs that provide power to the individual actuators. Both the motor boards and the main board possess a central processor, the Microchip PIC18F65J94 8-bit microcontroller. This microcontroller was chosen due to its high number of UART, USART, and I^2C channels, allowing for the accommodation of several peripheral inputs. These peripheral inputs to the main board provide valuable information to the control

system, ranging from navigation information to control inputs from the acoustic and optical communication modules. In addition to the microcontroller, the main board includes an MPU-9250 nine-axis inertial measurement unit and an Amphenol MEMs pressure sensor for state estimation. Altogether, these low-cost, low-power components create a highly adaptable control system that is able to act upon both environmental changes and external inputs (see Figure 6).

One of the major benefits of this embedded control system is its modularity. By constructing a modular design with the main control board physically isolated from the motor drive modules, the embedded system becomes easily expandable, requiring only additional driver PCBs rather than a complete system redesign to accommodate more motor outputs or sensor inputs. In addition, the modularity of the control system makes it resilient to single-motor or single-board failures, since the motor boards are low-cost and easily replaceable. Finally, each motor drive board has its own power supply input, allowing for individual batteries to provide power for individual sets of motors. This prevents the need for a single, high instantaneous current power supply that would be required if the entire system was to be operated on a single power rail.

Optical Communication System

Wireless underwater communication is necessary for certain AUV tasks. It is particularly important in a multi-AUV system for intervehicle communication, relative distance measurement, and vehicle navigation. We develop a compact optical communication system to supplement the acoustic communication system for the DAUV prototype. While the acoustic system, which is usually omnidirectional, addresses routine communication and exteroceptive sensing tasks, the optical communication system allows temporary, directional, high-speed transmission between the DAUVs and either the MAUVs or a docking station for large data packages.

One challenging yet critical task of multivehicle collaboration is the wireless communication between several interactive vehicles in a rapid but accurate manner. Conventionally, acoustic communication has served as the default means of underwater communication between collaborating vehicles. However, one of the major problems with acoustic communication is the data transmission rate, which for long-range systems is limited to tens of kilohertz (Heidemann et al., 2011). One promising wireless method for transmitting data is through the use of short-range, high-speed optical links. Many optical communication setups have already broken the Megabit per second (Mbps) barrier (Brundage, 2006; Simpson, 2007; Doniec et al., 2009). In this work, a 3-Mbps optical communication system is presented and tested in order to serve as a short-range link between the mother and daughter underwater vehicles.

The optical communication system is distributed into two sections: the transmitter and the receiver. The transmission source for the optical communication system was chosen to be a high-power CREE XRGRN 530 nm green LED, similar to that tested in Simpson (2007). This particular LED was chosen due to the fact that, in the visible electromagnetic spectrum, green (530 nm) light is one of the least attenuated wavelengths in water and would maximize transmission distance. The OPTX1006 collimating lens was attached to the transmitter PCB in order to reduce the divergence angle of light and further increase transmission distance. A high-speed IRF630 NFET was chosen to act as the high-current switch that activates the LEDs, driven by a TC4428 transistor driver. The input to the optical transmission system is an RS232 TTL logic signal for serial communication. By incorporating a single LED and collimating lens rather than a high-powered multi-LED or multilens array, this optical transmitter has been optimized for mobile platforms by significantly

FIGURE 6

Two major modules of the embedded control electronic system of the DAUV prototype.

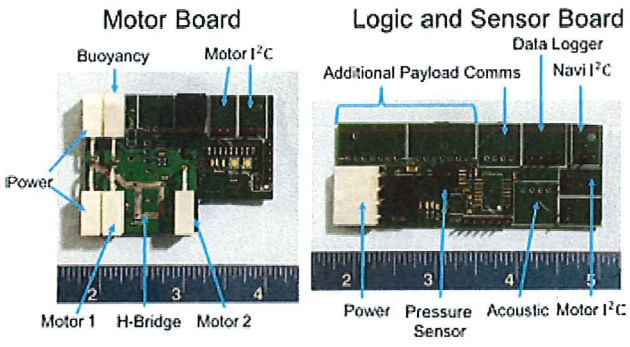

FIGURE 7

Rear and front views of optical transmitter PCB (a) and front view of optical receiver (b).

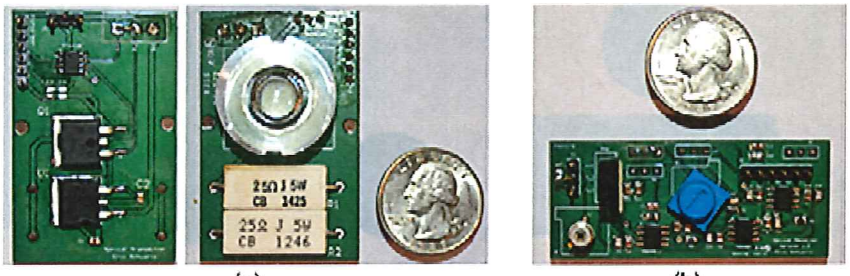

reducing the module size and power output. The optical transmitter hardware is shown in Figure 7a.

For the receiver circuit, shown in Figure 7b, a blue-green enhanced photodiode has been chosen as the optical detector in order to achieve the highest sensitivity to light when paired with the transmitter LED. The optical receiver circuit design is very similar to that presented by Brundage (2006) for high-speed underwater optical communication. However, in order to maximize the amount of radiant power received by the photodiode, the incoming light was focused through an LA1145-ML plano-convex lens from Thorlabs. This specific lens is suitable for mobile vehicle applications due to its relatively large size and short focal length, which is needed to preserve the compactness of the receiver module. The photodiode output current produced from the light beam is fed to a transimpedance amplifier, which converts the photodiode current into a voltage proportional to the value of the feedback resistor. The transimpedance amplifier output is further amplified and sent to a comparator along with a variable threshold voltage produced by an adjustable potentiometer.

The optical transmitter and receiver modules are integrated into the mother and daughter AUVs to test multivehicle communication using the underwater optical communication system. To model this underwater environment but still be able to readily adjust the transmitter and receiver position, a 1.22-m-long clear water tank was used as the medium of transmission for initial optical communication testing. To determine the maximum stable speed for the optical communication system, a function generator producing a pseudo-random binary sequence served as the input to the optical transmitter. After analyzing the degradation of the received waveform at increasing transmission speeds, it was concluded that the optical communication system could transmit and receive data at a rate of 3 Mbps while remaining stable. Transmission at these speeds would be more than sufficient for sending both control commands and real-time sensor or video data between collaborating vehicles.

In order to verify the stability of the 3-Mbps data rate during continuous data transfer, a single 100-kilobyte (kB) RGB image was transmitted across the medium. As seen in Figures 8a and 8b, the 100-kB image was able to be transmitted without error across the transmission medium, confirming the stability of the 3-Mbps transfer rate for our system. After performing this initial test, the phenomenon of temporary transfer interruption within the medium was investigated to determine its effect on the received data set. After the image transmission was halfway completed, an obstruction was inserted in front of the optical receiver for approximately 20% of the total transmission duration. As seen in Figure 8c, although image data was lost during the temporary blockage, it did not destabilize the system to the point where the post-blockage data was corrupted. This suggests that upon detecting either a signal blockage or transmitter-receiver misalignment, the data transmission can be paused and resumed when the condition has cleared, without corrupting the overall data transfer.

FIGURE 8

Optical communication testing of image transmission, including the original image (a), the received image at 3 Mbps (b), and the received image at 3 Mbps with the optical channel temporarily blocked during the transmission to emulate short-term transfer interruption due to misalignment or blockage (c).

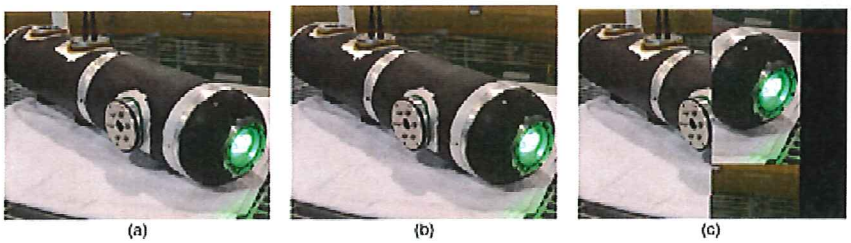

FIGURE 9

Underwater experiments of the DAUV prototype performing yaw, sway, and combined movements. Successive snapshots were taken at the labeled time steps. Engaged actuators are marked by arrows pointing in the direction of water flow movement. Lateral thruster motors were supplied with power at a 60% duty-cycle during these experiments.

Integrated Vehicle Testing

The maneuverability of the DAUV prototype was tested in a 60,000-gallon water tank as shown in the background of Figure 1b. This underwater testing environment is 26-foot in diameter and 15-foot deep. The DAUV prototype is fully actuated in horizontal motions, making it possible for us to experiment our multivehicle cooperation algorithms in a confined testing environment.

We first demonstrate the performance of the DAUV prototype with a series of typical maneuvering sequences. Figure 9 shows three vehicle movements including yaw, sway, and the combination of yaw and surge. Successive snapshots show the positions of the vehicle while the respective actuators (red arrows) were engaged. In this testing, all lateral thruster motors were supplied with power at a 60% duty-cycle. The zero-radius yaw movement was achieved by simultaneously actuating two thrusters on the diagonal. Such a movement was impossible for AUVs relying on control surfaces in tasks such as station-keeping and heading disturbance rejection. Even under a moderate thruster frequency setting, a 90-degree, zero-radius turn was achieved in about 3.5 s. The sway movement is another important feature enabled by our bioinspired thrusters that further improves the agility and controllability of the DAUV. Such maneuverability is extremely advantageous in tasks including autonomous docking or collision avoidance. During this experiment, the DAUV was able to translate in parallel for a body width in approximately 2.5 s. Finally, the combined motion with yaw and surge demonstrated in Figure 9 will be extremely beneficial in operations in a cluttered environment, such as inside a narrow pipe of a cooling system at a nuclear power plant or around fragile

FIGURE 10

Velocity profiles of the vehicle in surge (a), sway (b), and yaw (c) motions and the yaw velocity profile of the mother vehicle CephaloBot (d) for comparison purposes. Arrows indicate the direction of general flow movement when the corresponding actuator activates.

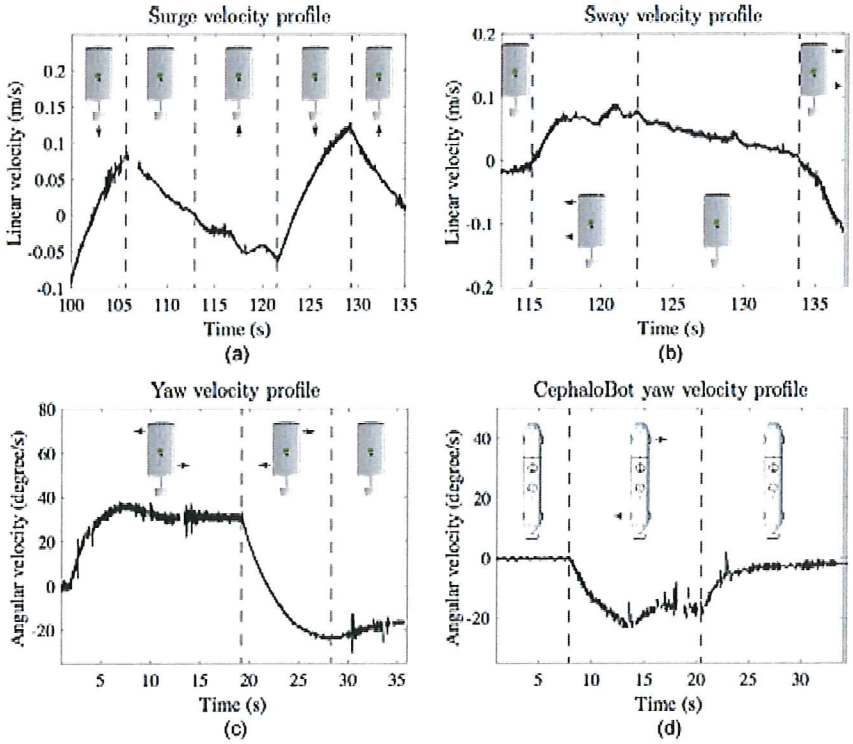

FIGURE 11

Vehicle's depth change responses in reaction to water volume increases in the buoyancy bag. A 100% full bag corresponds to approximately 3% vehicle weight increment. Initial descent was measured by the underwater motion capture system. Extrapolations of the measurement data show the rest of the steady-state vehicle descending movement before it reaches the bottom of the testing tank.

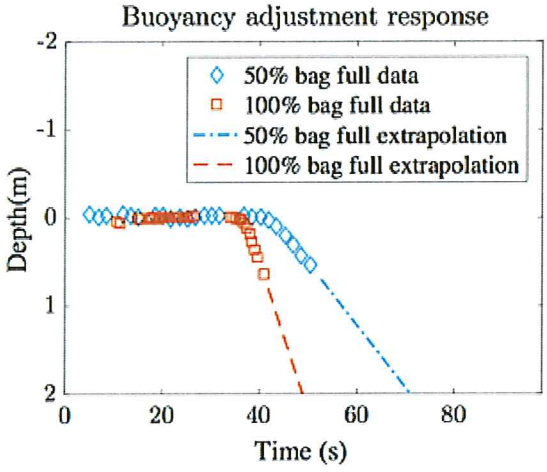

coral reefs. The combinations of all these movements constitute the high agility of the DAUV, enabling it to transit from one state to another both accurately and efficiently.

A closer evaluation of the maneuverability of the DAUV prototype is shown in Figures 10a-10c. During this testing, all actuators were operated at 100% power output. The velocity profiles are segmented into difference phases that correspond to different vehicle behaviors. The directions of general flow movements out of or through the vehicle thrusters are labeled for each phase to facilitate the interpretation of the vehicle's motion. We present filtered measurements by the underwater motion capture system. Oscillations and occasional data absences (such as in Figures 10a and 10c) are due to camera calibration residues and measurement noises of the underwater motion capture system caused by various factors such as room lighting and reflections on the water surface. Due to its small size, the DAUV prototype demonstrates faster response and higher agility in motion compared with CephaloBot. As shown in Figure 10d, the DAUV prototype has a higher steady-state yaw velocity, and it reaches this steady state value much faster than CephaloBot.

In order to illustrate the vehicle's dynamical response to buoyancy change controlled by the semiactive buoyancy compensation system, preliminary experiment results are shown in Figure 11. Two cases in which the vehicle was submerged were investigated with the buoyancy bag 50% full (1.5% vehicle weight increment) and 100% full (3% vehicle weight increment), respectively. Since the underwater motion capture system does not provide coverage beyond a certain depth (approximately 0.7 m) under current camera angle settings, only the measurement data of the initial descending phase are presented. Since the vehicle reaches steady state before it goes out of the measurable volume, extrapolation of the measured data reveals the rest of the descending motion. This has been validated based on the time that is measured independently for the vehicle to reach the bottom of our testing tank.

Finally, the practical performance of the optical communication system was evaluated with integrated vehicle

FIGURE 12

Experimental evaluation of the optical communication system while the vehicle is in motion. The numbers of successfully transmitted bits are reported under different relative velocities of the vehicle with respect to the optical receiver. Experimental data matches our prediction based on the theoretical model.

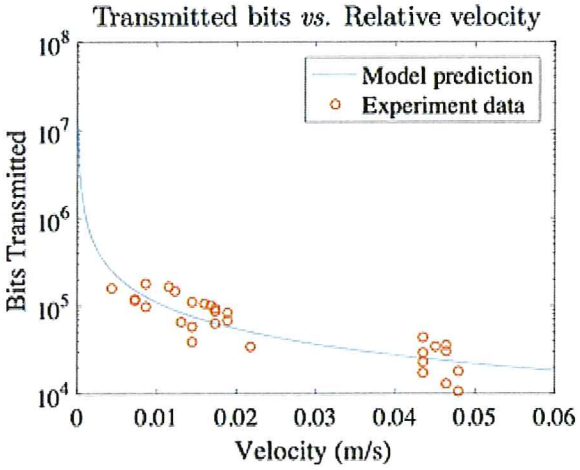

experiments, the results of which are shown in Figure 12. The transmitter was facing upward inside the top acrylic window of the DAUV, and the optical receiver was fixed facing downward with a vertical distance of 75 cm away from the vehicle plane. The yaw velocity of the vehicle was adjusted to emulate drive-by transmissions under various relative velocities between the transmitter and the receiver. A series of constant 10-bit characters were sent by the vehicle, and the numbers of received characters were logged and associated with the corresponding linear relative velocities calculated based on the vehicle's yaw velocities measured by the motion capture system. The experimental data matches our prediction based on the theoretic model, $N_{Bits} = \alpha * BR * 2(r_t + d \tan \theta_t)/v$ (Schwartz et al. 2016), where BR = 9,600 denotes the bit rate, r_t = 127 mm is the radius of the transmitter lens, d = 75 cm denotes the transmission distance, $\theta_t = 6°$ represents the transmission angle from the lens, v is the varying linear relative vehicle velocity, and α = 1/160 is a scaling factor that accounts for the transmission overhead due to the embedded program execution time and UART transmission delays.

Conclusion

In this article, we presented the design of a cost-effective, compact AUV prototype, dubbed the DAUV, for testing a mother-daughter, multivehicle collaboration hierarchy together with our previous AUV design, CephaloBot (Krieg et al., 2011). The DAUV is equipped with a set of improved jet thrusters that were inspired by the locomotion of squid and jellyfish. These thrusters enable fully decoupled rotational and lateral movements and remove the necessity of control surfaces without sacrificing the hydrodynamic efficiency of the vehicle. High maneuverability was achieved, allowing more precise and efficient control of the vehicle motion. A semiactive buoyancy control system, inspired by the buoyancy system of the nautilus, was developed to adjust the vehicle depth.

To overcome the challenges that arise when decreasing the vehicle dimension while still preserving essential capabilities, we adopted 3D printing technology in manufacturing the daughter vehicle prototype. This significantly reduced the fabrication time compared to conventional subtractive manufacturing techniques and allowed the creation of more complex structures to better utilize the limited internal space. We commented on several practical issues that require special care in the adoption of 3D printing technology in underwater vehicle fabrication.

A compact embedded control system was custom-designed to provide necessary actuation and sensing capabilities required for multivehicle interaction in our indoor testing environment. This system features a modular design for distributed placement inside the vehicle as well as for simplicity of debugging and system expansion. To supplement the acoustic communication system, the DAUV prototype showcases a compact, optical communication modem that handles short-range, high-speed transmission of large data packages.

Although the development of the DAUV prototype achieved success, several improvements were identified to simplify the manufacturing process and enhance the vehicle stability in future development. We are currently improving the vehicle's structural design to better integrate 3D printing materials and metal materials for easy vehicle sealing. A more space-efficient internal structure design is also under investigation for the vehicle to house a more capable embedded electronic system. Multiple DAUVs will be fabricated to constitute a multi-AUV experimental setup for our collaborative control and state estimation algorithms.

Acknowledgment

The authors would like to thank the Office of Naval Research for funding this project.

Corresponding Author:

Kamran Mohseni
University of Florida, Room 141 NEB
Gainesville, FL 32611-6250
Email: mohseni@ufl.edu

References

Anderson, E.J., & DeMont, M.E. 2000. The mechanics of locomotion in the squid *Loligo pealei*: Locomotory function and unsteady hydrodynamics of the jet and intramantle pressure. J Exp Biol. 203(18):2851-63.

Bahr, A., Leonard, J.J., & Fallon, M.F. 2009. Cooperative localization for autonomous underwater vehicles. Int J Robot Res. 28(6):714-28. http://dx.doi.org/10.1177/0278364908100561.

Bartol, I.K., Krueger, P.S., Thompson, J.T., & Stewart, W.J. 2008. Swimming dynamics and propulsive efficiency of squids throughout ontogeny. ICB. 48(6):720-33. http://dx.doi.org/10.1093/icb/icn043.

Bartol, I.K., Krueger, P.S., Stewart, W.J., & Thompson, J.T. 2009. Hydrodynamics of pulsed jetting in juvenile and adult brief squid *Lolliguncula brevis*: Evidence of multiple jet 'modes' and their implications for propulsive efficiency. J Exp Biol. 212(12):1889-903. http://dx.doi.org/10.1242/jeb.027771.

Brundage, H. 2006. Designing a wireless underwater optical communication system. Master's thesis, Massachusetts Inst. Technol., Cambridge, MA, USA.

Chao, Y., Li, Z., Farrara, J.D., Moline, M.A., Schofield, O.M.E., & Majumdar, S.J. 2008. Synergistic applications of autonomous underwater vehicles and the regional ocean modeling system in coastal ocean forecasting. Limnol Oceanogr. 53(5part2):2251-63. http://dx.doi.org/10.4319/lo.2008.53.5_part_2.2251.

Clark, C.M., Forney, C., Manii, E., Shinzaki, D., Gage, C., Farris, M., ... Moline, M. 2013. Tracking and following a tagged leopard shark with an autonomous underwater vehicle. J Field Robotics. 30(3):309-22. http://dx.doi.org/10.1002/rob.21450.

Chu, W.S., Lee, K.T., Song, S.H., Han, M.W., Lee, J.Y., Kim, H.S., ... Ahn, H.S. 2012. Review of biomimetic underwater robots using smart actuators. Int J Precis Eng Man. 13(7):1281-92. http://dx.doi.org/10.1007/s12541-012-0171-7.

Dabiri, J.O., Colin, S.P., Costello, J.H., & Gharib, M. 2005. Flow patterns generated by oblate medusan jellyfish: Field measurements and laboratory analyses. J Exp Biol. 208:1257-65. http://dx.doi.org/10.1242/jeb.01519.

Dabiri, J.O., Colin, S.P., Katija, K., & Costello, J.H. 2010. A wake-based correlate of swimming performance and foraging behavior in seven co-occurring jellyfish species. J Exp Biol. 213:1217-25. http://dx.doi.org/10.1242/jeb.034660.

D'Asaro, E.A. 2003. Performance of autonomous Lagrangian floats. J Atmos Ocean Technol. 20:896-911. http://dx.doi.org/10.1175/1520-0426(2003)020<0896:POALF>2.0.CO;2.

Das, J., Py, F., Maughan, T., O'Reilly, T., Messié, M., Ryan, J., ... Rajan, K. 2012. Coordinated sampling of dynamic oceanographic features with underwater vehicles and drifters. Int J Robot Res. 31(5):626-46. http://dx.doi.org/10.1177/0278364912440736.

DeVries, L., Lagor, F.D., Lei, H., Tan, X., & Paley, D.A. 2015. Distributed flow estimation and closed-loop control of an underwater vehicle with a multi-modal artificial lateral line. Bioinspir Biomim. 10(2):025002. http://dx.doi.org/10.1088/1748-3190/10/2/025002.

Doniec, M., Vasilescu, I., Chitre, M., Detweiler, C., Hoffmann-Kuhnt, M., & Rus, D. 2009. AquaOptical: A lightweight device for high-rate long-range underwater point-to-point communication. In: OCEANS 2009. Biloxi, MS: MTS/IEEE.

Eriksen, C.C., Osse, T.J., Light, R.D., Wen, T., Lehman, T.W., Sabin, P.L., ... Chiodi, A.M. 2001. Seaglider: A long-range autonomous underwater vehicle for oceanographic research. IEEE J Ocean Eng. 26(4):424-36. http://dx.doi.org/10.1109/48.972073.

Fernandes, P.G., Brierley, A.S., Simmonds, E.J., Millard, N.W., McPhail, S.D., Armstrong, F., ... Squires, M. 2000. Oceanography: Fish do not avoid survey vessels. Nature. 404:35-6. http://dx.doi.org/10.1038/35003648.

Fossen, T.I. 1994. Guidance and Control of Ocean Vehicles. Hoboken, NJ: Wiley-Interscience. 494 pp.

Gharib, M., Rambod, E., & Shariff, K. 1998. A universal time scale for vortex ring formation. J Fluid Mech. 360:121-40. http://dx.doi.org/10.1017/S0022112097008410.

Giorgio-Serchi, F., Arienti, A., & Laschi, C. 2016. Underwater soft-bodied pulsed-jet thrusters: Actuator modeling and performance profiling. Int J Robot Res. 35(11):1308-29. http://dx.doi.org/10.1177/0278364915622569.

Grasmueck, M., Eberli, G.P., Viggiano, D.A., Correa, T., Rathwell, G., & Luo, J. 2006. Autonomous underwater vehicle (AUV) mapping reveals coral mound distribution, morphology, and oceanography in deep water of the Straits of Florida. Geophys Res Lett. 33:L23616. http://dx.doi.org/10.1029/2006GL027734.

Heidemann, J., Stojanovic, M., & Zorzi, M. 2011. Underwater sensor networks: Applications, advances and challenges. Philos Trans A Math Phys Eng Sci. 370:158-75. http://dx.doi.org/10.1098/rsta.2011.0214.

Howe, B., Chao, Y., Arabshahi, P., Roy, S., McGinnis, T., & Gray, A. 2010. A smart sensor web for ocean observation: Fixed and mobile platforms, integrated acoustics, satellites and predictive modeling. IEEE J Sel Topics Appl Earth Observ Remote Sens. 3(4):507-21. http://dx.doi.org/10.1109/JSTARS.2010.2052022.

Krieg, M., & Mohseni, K. 2008. Thrust characterization of pulsatile vortex ring generators for locomotion of underwater robots. IEEE J Ocean Eng. 33(2):123-32. http://dx.doi.org/10.1109/JOE.2008.920171.

Krieg, M., & Mohseni, K. 2010. Dynamic modeling and control of biologically inspired vortex ring thrusters for underwater robot locomotion. IEEE Trans Robot 26(3):542-54. http://dx.doi.org/10.1109/TRO.2010.2046069.

Krieg, M., Klein, P., Hodgkinson, R., & Mohseni, K. 2011. A hybrid class underwater vehicle: Bioinspired propulsion, embedded system, and acoustic communication and localization system. Mar Technol Soc J. 45(4):153-64. http://dx.doi.org/10.4031/mtsj.45.4.11.

Krieg, M., & Mohseni, K. 2013. Modelling circulation, impulse and kinetic energy of starting jets with non-zero radial velocity. J Fluid Mech. 719:488-526. http://dx.doi.org/10.1017/jfm.2013.9.

Krieg, M., Sledge, I.J., & Mohseni, K. 2015. Design considerations for an underwater soft-robot inspired from marine invertebrates. Bioinspir Biomim. 10(6):065004. http://dx.doi.org/10.1088/1748-3190/10/6/065004.

Krieg, M., & Mohseni, K. 2015. Pressure and work analysis of unsteady, deformable, axisymmetric, jet producing cavity bodies. J Fluid Mech. 769:337-68. http://dx.doi.org/10.1017/jfm.2015.120.

Leonard, N.E., Paley, D.A., Lekien, F., Sepulchre, R., Fratantoni, D.M., & Davis, R.E. 2007. Collective motion, sensor net3-work, and ocean sampling. Proc IEEE. 95(1):48-74. http://dx.doi.org/10.1109/JPROC.2006.887295.

Lighthill, M.J. 1969. Hydrodynamics of aquatic animal locomotion. Annu Rev Fluid Mech. 1:413-45. http://dx.doi.org/10.1146/annurev.fl.01.010169.002213.

Lipinski, D., & Mohseni, K. 2009. Flow structures and fluid transport for the hydromedusae *Sarsia tubulosa* and *Aequorea victoria*. J Exp Biol. 212:2436-47. http://dx.doi.org/10.1242/jeb.026740.

Michini, M., Hsieh, M.A., Forgoston, E., & Schwartz, I.B. 2014. Robotic tracking of coherent structures in flows. IEEE Trans Robot. 30(3):593-603. http://dx.doi.org/10.1109/TRO.2013.2295655.

Mohseni, K. 2006. Pulsatile vortex generators for low-speed maneuvering of small underwater vehicles. Ocean Eng. 33(16):2209-23. http://dx.doi.org/10.1016/j.oceaneng.2005.10.022.

Palmre, V., Hubbard, J.J., Fleming, M., Pugal, D., Kim, S., Kim, K.J., & Leang, K.K. 2013. An IPMC-enabled bio-inspired bending/twisting fin for underwater applications. Smart Mater Struct. 22(1):014003. http://dx.doi.org/10.1088/0964-1726/22/1/014003.

Reed, B., & Hover, F. 2014. Oceanographic pursuit: Networked control of multiple vehicles tracking dynamic ocean features. Methods Oceanogr. 10:21-43. http://dx.doi.org/10.1016/j.mio.2014.05.001.

Roemmich, D. & the Argo Steering Team. 2009. Argo: The challenge of continuing 10 years of progress. Oceanography. 22(3):46-55. http://dx.doi.org//10.5670/oceanog.2009.65.

Sahin, M., & Mohseni, K. 2009. An arbitrary Lagrangian-Eulerian formulation for the numerical simulation of flow patterns generated by the hydromedusa *Aequorea victoria*. J Comput Phys. 228(12):4588-605. http://dx.doi.org/10.1016/j.jcp.2009.03.027.

Schwartz, E., Song, Z., Chen, R., & Mohseni, K. 2016. Low-power optical communication for compact autonomous underwater vehicles (Submitted for publication).

Sledge, I.J., Krieg, M., Lipinski, D., & Mohseni, K. 2015. Identifying and modeling motion primitives for the hydromedusae Sarsia tubulosa and Aequorea victoria. Bioinspir Biomim. 10(6):066001. http://dx.doi.org/10.1088/1748-3190/10/6/066001.

Simpson, J. 2007. A 1 Mbps underwater communications system using LEDs and photodiodes with signal processing capability. Master's thesis, North Carolina State University, Raleigh, NC, USA.

Song, Z., & Mohseni, K. 2013. Hierarchical underwater localization in dominating background flow fields. In: IROS 2013. 3356-61. Tokyo, Japan: IEEE/RSJ.

Song, Z., & Mohseni, K. 2014. A distributed localization hierarchy for an AUV swarm. In: ACC 2014. 4721-26. Portland: IEEE. http://dx.doi.org/10.1109/acc.2014.6859344.

Weymouth, G.D., Subramaniam, V., & Triantafyllou, M.S. 2015. Ultra-fast escape maneuver of an octopus-inspired robot. Bioinspir Biomim. 10(1):016016. http://dx.doi.org/10.1088/1748-3190/10/1/016016.

Xu, Y., & Mohseni, K. 2014. Bio-inspired hydrodynamic force feed forward for autonomous underwater vehicle control. IEEE/ASME Trans Mechatronics. 4(19):1127-37. http://dx.doi.org/10.1109/TMECH.2013.2271037.

Yoerger, D., Cooke, J., & Slotine, J.J. 1990. The influence of thruster dynamics on underwater vehicle behavior and their incorporation into control system design. IEEE J Ocean Eng. 15(3):167-78. http://dx.doi.org/10.1109/48.107145.